

# Smart nanoprobes for ultrasensitive detection of breast cancer via magnetic resonance imaging

Jaemin Lee<sup>1</sup>, Jaemoon Yang<sup>1,2</sup>, Sung-Baek Seo<sup>1,3</sup>, Hyun-Ju Ko<sup>2</sup>, Jin-Suck Suh<sup>2</sup>, Yong-Min Huh<sup>2,4</sup> and Seungjoo Haam<sup>1,4</sup>

<sup>1</sup> Department of Chemical and Biomolecular Engineering, College of Engineering, Yonsei University, Seoul 120-749, Korea

<sup>2</sup> Department of Radiology, College of Medicine, Yonsei University, Seoul 120-752, Korea

<sup>3</sup> Yonsei Nanomedical National Core Research Center, Seoul 120-749, South Korea

E-mail: [jpmi01@yonsei.ac.kr](mailto:jpmi01@yonsei.ac.kr), [177hum@yonsei.ac.kr](mailto:177hum@yonsei.ac.kr), [ssjy8199@hotmail.com](mailto:ssjy8199@hotmail.com), [ok6336@hanmail.net](mailto:ok6336@hanmail.net), [jss@yumc.yonsei.ac.kr](mailto:jss@yumc.yonsei.ac.kr), [ymhuh@yumc.yonsei.ac.kr](mailto:ymhuh@yumc.yonsei.ac.kr) and [haam@yonsei.ac.kr](mailto:haam@yonsei.ac.kr)

Received 17 August 2008, in final form 28 September 2008

Published 11 November 2008

Online at [stacks.iop.org/Nano/19/485101](http://stacks.iop.org/Nano/19/485101)

## Abstract

Antibody-conjugated hydrophilic magnetic nanocrystals for use as smart nanoprobes were developed for ultrasensitive detection of breast cancer via magnetic resonance (MR) imaging.  $\text{MnFe}_2\text{O}_4$  nanocrystals (MNCs) for use as MR imaging contrast agents were synthesized by thermal decomposition to take advantage of their MR signal enhancement effect. The MNC surfaces were then modified with amphiphilic tri-block copolymers (dicarboxy poly(ethylene glycol)-block-poly(propylene glycol)-block-poly(ethylene glycol)), not only allowing the MNCs to transfer from the organic to the aqueous phase, but also increasing the colloidal stability of the MNCs by masking poly(ethylene glycol). The physicochemical properties of the synthesized hydrophilic magnetic nanocrystals (HMNCs) were fully investigated. Trastuzumab (TZ), a monoclonal antibody against human epidermal growth factor receptor (HER2/neu), was further conjugated on the surface of HMNCs to specifically target HER2/neu over-expressed breast cancer cells. MR imaging analysis of target cells treated with TZ-conjugated HMNCs (TZ-HMNCs) clearly demonstrated their potential as high-performance nanoprobes for selective imaging.

(Some figures in this article are in colour only in the electronic version)

## 1. Introduction

Magnetic resonance (MR) imaging is a powerful technology with widespread application in medicine, including cancer diagnosis [1–7]. MR imaging techniques have been greatly improved by the availability of better MR contrast agents with increasing monodispersity and magnetic sensitivity [8–10]. Recently, hydrophobic magnetic nanocrystals synthesized by thermal decomposition in organic solution have been considered an emerging substance because of their very well-defined crystalline structure, stoichiometry, and magnetism,

with a narrow size distribution compared to magnetic nanocrystals prepared in the aqueous phase [11–19]. Due to the hydrophobic ligands such as fatty acids on the surface of crystal structure, however, thermally decomposed magnetic nanocrystals have low colloidal stability in the aqueous phase. In order to apply magnetic nanocrystals as MR contrast agents for biomedical imaging, therefore, the formulation of highly water-dispersible magnetic nanocrystals is essential. In general, there are two main strategies to increase solubility in an aqueous medium; one is the exchange of hydrophobic surface ligands with hydrophilic agents (exchange method), and the other is wrapping of

<sup>4</sup> Authors to whom any correspondence should be addressed.

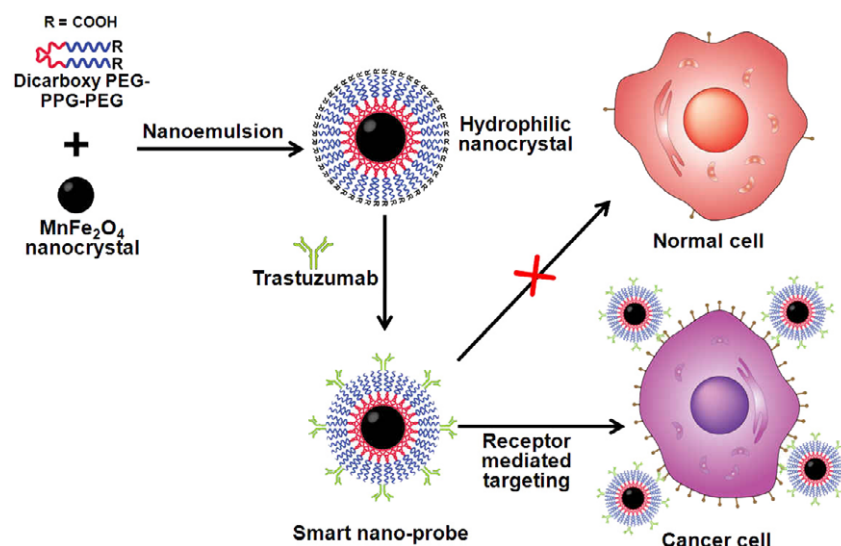


**Figure 1.** Schematic illustration of TZ-HMNCs for the detection of HER2/neu over-expressed breast cancer by MR imaging. Highly stable hydrophilic nanocrystals (HMNCs) were prepared by a nanoemulsion method using dicarboxy PEG–PPG–PEG and  $\text{MnFe}_2\text{O}_4$  nanocrystals. The HMNCs were further modified by the anti-HER2/neu antibody, Trastuzumab (TZ).

hydrophobic magnetic nanocrystals using amphiphilic agents (addition method) [20–24]. For example, ligand-exchanged water-dispersible magnetic nanocrystals as MR contrast agents were first introduced by Cheon and co-workers [25]. These MR contrast agents for *in vivo* monitoring of molecular and cellular events demonstrate low toxicity and excellent sensitivity under magnetic fields [25]. However, the colloidal stability of these water-dispersible magnetic nanocrystals was maintained only within a narrow range of salt concentrations and pH conditions since the exchanged hydrophilic ligand was relatively short. Thus, magnetic nanocrystals covered with a long chain of amphiphilic block copolymers represent one approach to increase the aqueous solubility and stability [26]. Peculiarly, the addition of poly(ethylene glycol)-based block copolymers with high molecular weight can enhance the colloidal stability and increase the blood half-life by rendering the protein non-immunogenic and non-antigenic [27, 28]. Furthermore, the synthesis of water-dispersible magnetic nanocrystals using the addition method is quite simple and beneficial for loading biomolecules such as genes or drugs [20, 29–31]. For this purpose, the use of poly(ethylene glycol)-block-poly(propylene glycol)-block-poly(ethylene glycol) (PEG–PPG–PEG), a tri-block copolymer (commercial name Pluronic® F127), is one suitable approach for phase transfer agents [32, 33]. The hydroxyl groups at the end of PEG–PPG–PEG can be activated or modified by bioconjugation chemistry, further facilitating their direct conjugation to amine-containing antibodies or peptides for tumor-specific detection [34].

Herein, we report the formulation of systemic smart nanoprobes with antibody-conjugated hydrophilic magnetic nanocrystals (HMNCs) using PEG–PPG–PEG for breast cancer detection. For the preparation of high-quality MR imaging agents, we first synthesized monodisperse  $\text{MnFe}_2\text{O}_4$  nanocrystals (MNCs). Subsequently, the phase transference of hydrophobic MNCs toward the aqueous phase was achieved

by a nanoemulsion method using dicarboxy PEG–PPG–PEG as a stabilizer [22]. To assess the potential as nanoprobes, the morphology, size distribution, colloidal stability, and chemical compositions of the HMNCs were analyzed. In order to detect specific cancerous parts via MR imaging, anti-HER2/neu monoclonal antibody (Trastuzumab, TZ) as a breast cancer targeting moiety was further conjugated on the surface of HMNCs (TZ-HMNCs). In addition, the biocompatibility and cellular targeting efficacy of TZ-HMNCs were fully evaluated. The conceptual scheme of TZ-HMNCs is depicted in figure 1.

## 2. Materials and methods

### 2.1. Materials

Iron (III) acetylacetonate, manganese (II) acetylacetonate, 1,2-hexadecanediol, oleic acid, oleylamine, benzyl ether, poly(ethylene glycol)-poly(propylene glycol)-poly(ethylene glycol) (PEG–PPG–PEG,  $M_w$ : 12 600 Da), succinic anhydride (SA), 4-dimethylaminopyridine (DMAP), triethylamine, 1,4-dioxane and *N*-(3-dimethylaminopropyl)-*N*-ethylcarbodiimide hydrochloride (EDC) were purchased from Sigma-Aldrich. *N*-hydroxysulfosuccinimide (sulfo-NHS) was purchased from Pierce. Trastuzumab (TZ) was purchased from F. Hoffmann–La Roche Ltd. Phosphate buffered saline (PBS; 10 mM, pH 7.4) was purchased from Gibco. All other chemicals and reagents were of analytical grade.

### 2.2. Synthesis of $\text{MnFe}_2\text{O}_4$ nanocrystals (MNCs)

Monodisperse  $\text{MnFe}_2\text{O}_4$  nanocrystals (MNCs) were synthesized by a thermal decomposition method using magnetic acetylacetonates as precursors [17, 18]. 2 mmol of iron (III) acetylacetonate, 1 mmol of manganese (II) acetylacetonate, 10 mmol of 1,2-hexadecanediol, 6 mmol of oleic acid, 6 mmol



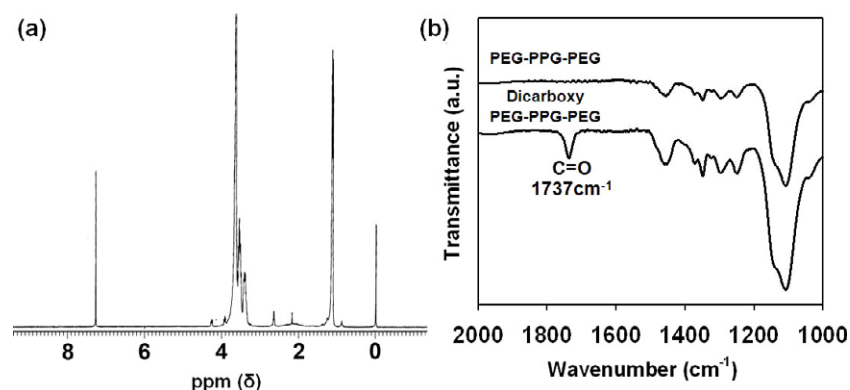


**Figure 3.** (a)  $^1\text{H}$ -NMR spectra of dicarboxy PEG-PPG-PEG. (b) FT-IR spectra of PEG-PPG-PEG and dicarboxy PEG-PPG-PEG.

microscope (HR-TEM, JEM-2100F, JEOL Ltd). The amounts of iron and manganese ions were measured by ICP-OES (IRIS Intrepid II XDL, Thermo Elemental). The magnetic hysteresis loop and saturation of magnetization were obtained using a vibrating sample magnetometer (MODEL-7300, Lakeshore). X-ray diffraction patterns of the HMNCs were obtained with a Rigaku D/max-RB (Tokyo, Japan) powder diffractometer and by image-plate photography using graphite-monochromatized Cu K $\alpha$  radiation ( $\lambda = 1.542 \text{ \AA}$ ). Data were collected from  $20^\circ$  to  $80^\circ$  with a step size of  $0.05^\circ$  and an interval of 5 s.

## 2.7. Cytotoxicity test for HMNCs

For evaluation of the cytotoxicity by HMNCs, HER2/neu receptor over-expressed NIH3T6.7 cells and NIH3T3 cells as normal cells were selected (American Type Culture Collection, Manassas, VA). The cells were maintained in DMEM (Gibco, NY, USA), containing 10% (v/v) fetal bovine serum,  $100 \text{ U ml}^{-1}$  penicillin, and  $0.1 \text{ mg ml}^{-1}$  streptomycin in a 5%  $\text{CO}_2$  humidified atmosphere at  $37^\circ\text{C}$ . The cytotoxicity for HMNCs was then evaluated by measuring the inhibition of cell growth using an MTT assay. Briefly, the cells were plated at a density of  $4 \times 10^3 \text{ cells ml}^{-1}$  in 96-well plates and treated with HMNCs at various concentrations ( $10^{-3}$ – $1 \text{ mg ml}^{-1}$ ) for 72 h. The cell viabilities were then obtained by calculating the ratio of the number of viable cells in the treated culture compared with non-treated control cells.

## 2.8. Targeting efficacy of TZ-HMNCs against cancer cells

The targeting efficacy of TZ-HMNCs as smart nanoprobes for cancer cells was investigated by microscopy and MR imaging. The cells ( $1 \times 10^6 \text{ cells/well}$ ) were incubated with TZ-HMNCs ( $43 \text{ \mu g ml}^{-1}$ ) at  $4^\circ\text{C}$  for 4 h and then they were washed twice with PBS (pH 7.4, 10 mM). Subsequently, TZ-HMNC treated cells were incubated with fluoroisothiocyanate-labeled goat anti-human Immunoglobulin G in previously described media at  $37^\circ\text{C}$  for 4 h. The cells were washed twice with PBS (pH 7.4, 10 mM) and were collected by trypsinization. Finally, the samples were washed three times with 0.2% fetal bovine serum and 0.02%  $\text{NaN}_3$  in PBS (pH 7.4, 10 mM) and re-suspended in  $400 \text{ \mu L}$  of paraformaldehyde (4%).

Scanning of the cell-associated fluorescence was performed using FACScalibur equipment (Beckton-Dickinson, Mansfield, MA) at the wavelength of 488 nm. The specific binding and cellular uptake of prepared nanoparticles were visualized by confocal microscopy (LSM 510, Olympus, Tokyo, Japan). Moreover, the cellular uptake efficiency of TZ-HMNCs was also examined by the Prussian blue staining method against both NIH3T3 and NIH3T6.7 cells.

MR imaging of the HMNC solutions and model cells treated with TZ-HMNCs was performed with a 1.5 T clinical MR imaging instrument with a micro-47 surface coil (Intera; Philips Medical Systems, Best, The Netherlands). For T2 (spin-spin relaxation time)-weighted MR imaging of *in vitro* cells at 1.5 T, the following parameters were adopted: point resolution =  $156 \text{ \mu m} \times 156 \text{ \mu m}$ , section thickness = 0.6 mm, TE (time to repeat) = 60 ms, TR (echo time) = 4000 ms, number of acquisitions = 1.

## 2.9. Statistical analysis

All experiments were performed in triplicate and the values were expressed as average  $\pm$  standard deviation. The two-tailed Student's *t*-test was used to assess if the difference in relative T2 weight value and relative fluorescence intensity between the treated group and the non-treated group was significant.  $p < 0.05$  was considered to be statistically significant [36].

## 3. Results and discussion

To prepare HMNCs as smart imaging agents, the hydroxyl group of PEG-PPG-PEG was modified with carboxyl group by an esterification process using SA. The terminal carboxyl group of dicarboxylated PEG-PPG-PEG can be easily conjugated with the amine group of the targeting moiety. Moreover, phase transfer of hydrophobic MNCs with HMNCs was successfully achieved by the addition of dicarboxylated PEG-PPG-PEG against the surface of MNCs due to the amphiphilic properties. After modification of the functional group, the chemical structure of the dicarboxylated PEG-PPG-PEG was evaluated by  $^1\text{H}$ -NMR; the characteristic peaks are presented in figure 3(a). The  $\delta$  values were 1.14 ppm



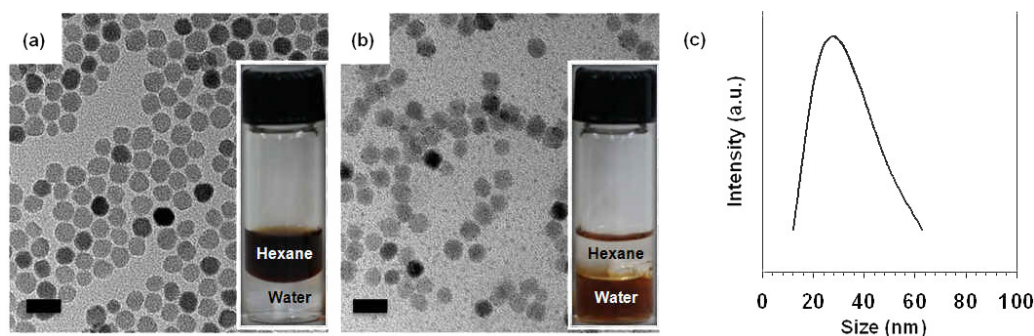


**Figure 4.** TEM images of (a) MNCs in hexane and (b) HMNCs in water; inset: solubility test against MNCs and HMNCs. The scale bars represent 20 nm. (c) Size distribution of HMNCs determined by laser scattering.

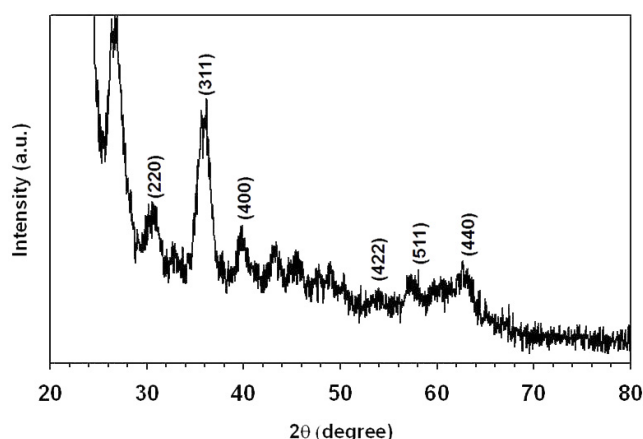


**Figure 5.** X-ray diffraction pattern of HMNCs. The x-ray diffraction patterns match the literature values for stoichiometric  $\text{MnFe}_2\text{O}_4$  (JCPDS No. 10-319).

( $-\text{CH}_3$  of PPG chains) and 3.64 ppm ( $-\text{CH}_2-$  of PEG chains and  $-\text{CH}-$  of PPG chains), respectively. In addition, the chain ( $-\text{CH}_2\text{CH}_2-$ ) generated by SA was verified at 2.55 ppm. We further confirmed the characteristic band of dicarboxylated PEG-PPG-PEG using FT-IR spectra (figure 3(b)). The anhydride group of SA ( $1783$  and  $1861\text{ cm}^{-1}$ ) was converted to a carboxyl group ( $1737\text{ cm}^{-1}$ ) after esterification of the hydroxyl group of PEG-PPG-PEG by the ring opening process of SA. These results demonstrate that dicarboxylated PEG-PPG-PEG was successfully synthesized.

Monodisperse MNCs ( $\text{MnFe}_2\text{O}_4$ ) of size 10 nm were synthesized by a seed-mediated growth method [18]. The morphology of the MNCs as revealed by TEM is shown in figure 4(a). The MNCs were dispersed in non-polar organic solvents and they were not dispersible in the aqueous phase because of the oleic acid on the surface of the MNCs (inset of figure 4(a)). To increase the colloidal stability against the aqueous phase, dicarboxylated PEG-PPG-PEG was introduced to coat the MNC surfaces. Due to the hydrophobic interaction of MNCs with the PPG chains of the amphiphilic dicarboxylated PEG-PPG-PEG, HMNCs were successfully prepared by a nanoemulsion method (figure 4(b)). Therefore, the MNCs were well dispersed in the aqueous phase due to the spontaneous PEGylation by hydrophilic

PEG chains (inset of figure 4(b)). The size distribution of HMNCs was determined by light scattering to be  $29 \pm 10$  nm (figure 4(c)). Furthermore, the presence of  $\text{MnFe}_2\text{O}_4$  nanocrystals in the HMNCs was verified from the x-ray diffraction pattern. Although  $\text{MnFe}_2\text{O}_4$  nanocrystals were covered with organic components, the spinel structure of the nanocrystals was maintained (figure 5).

Colloidal stability of HMNCs is an essential requirement for application as MR probes. We thus examined the colloidal stability of HMNCs for a wide range of pHs and various concentrations of salt. As shown in figure 6, the HMNCs ( $7.5\text{ mg ml}^{-1}$ ) demonstrated excellent colloidal stability for various pHs (4–13). Furthermore, the HMNCs were not aggregated or precipitated even at high salt concentrations ( $\text{NaCl}$ ;  $0.1$ – $1\text{ M}$ ) because the PEG chains on the surface of the HMNCs prevented them from attack by ions and change of proton concentration [27, 28].

We next investigated the magnetic properties and induced MR signals of HMNCs as contrast agents to better understand the diagnostic potential. T2-weighted spin-echo MR imaging of HMNCs displayed a significant shift in lower signal intensity along with increasing HMNCs concentration (figure 7(a)). Red color (rightmost map image) means high MR intensity and blue color (leftmost map image) is low MR intensity. The relaxivity of HMNCs containing  $\text{MnFe}_2\text{O}_4$  nanocrystals increased linearly according to increase of the HMNC concentration; the relaxivity coefficient was  $236\text{ l mmol}^{-1}\text{ s}^{-1}$  (figure 7(b)). Magnetic hysteresis loops of HMNCs were observed using a vibration sample magnetometer at 300 K (figure 7(c)), revealing that the HMNCs exhibited superparamagnetic behavior without magnetic hysteresis. The saturation of magnetization value for HMNCs was  $1.56\text{ emu g}^{-1}$  at 0.85 T. These results demonstrated that HMNCs have potential as MR imaging agents.

The *in vitro* cytotoxic activity of HMNCs for model cells was measured by MTT assay (figure 8). Cell viability was observed after cells were exposed to various concentrations ( $10^{-3}$ – $1\text{ mg ml}^{-1}$ ) of HMNCs for 72 h. Within the concentration range of  $10^{-3}$ – $1\text{ mg ml}^{-1}$ , the viability of both cells was maintained at more than 85%. Therefore, the HMNCs were biocompatible and revealed the possibility of use as nanoprobes for cancer detection.

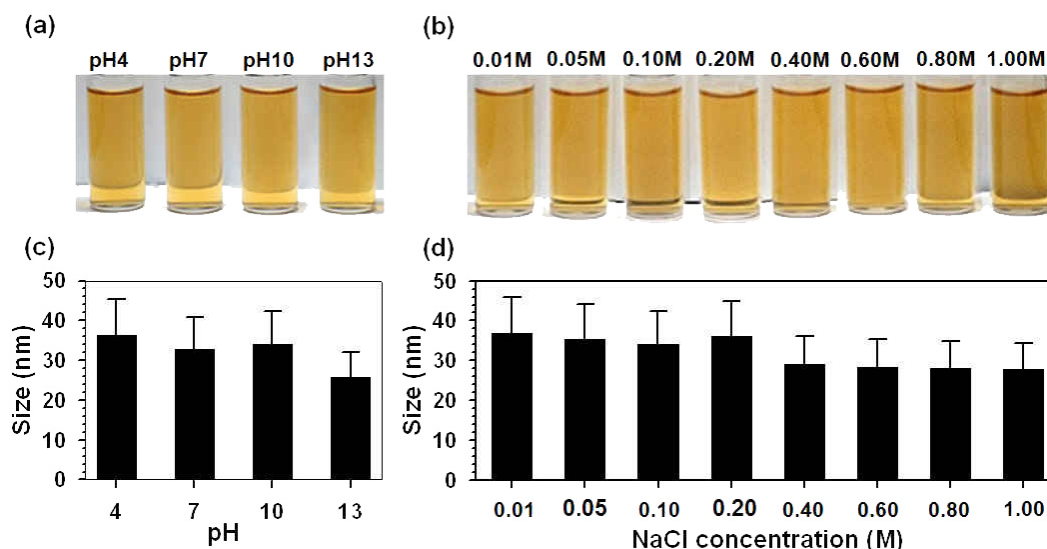


**Figure 6.** Colloidal stability test of HMNCs against various (a) pHs and (b) NaCl concentrations. Size analysis of HMNCs against various (c) pHs and (d) NaCl concentrations; average  $\pm$  standard deviation.

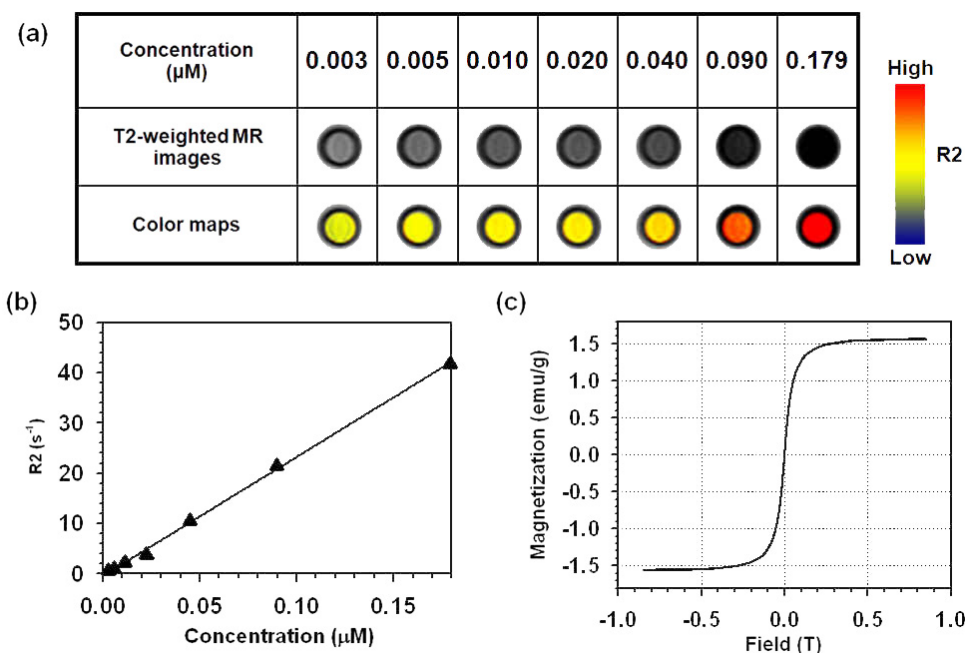


**Figure 7.** (a) Concentration-dependent T2-weighted MR images of HMNCs in aqueous solution, (b) graph of relaxivity versus the concentration of HMNCs, and (c) the magnetic hysteresis loop of HMNCs obtained with a vibration sample magnetometer at 300 K.

The specific targeting efficacy of antibody-conjugated HMNCs (TZ-HMNCs) against cancer cell lines was evaluated using fluorescence activated cell sorting (FACS) analysis. The receptor, HER2/neu, is over-expressed for patients with metastatic breast cancer; this serves as a tumor-targeting marker for the treatment. TZ has been attached at the HER2/neu receptor and it obstructs the binding of growth factors, which inhibit the phosphorylation process. In addition, TZ inhibits the growth and proliferation of breast cancer cells. Thus, TZ was conjugated with HMNCs for proof of concept. 16 equivalent Trastuzumab were conjugated on surface of HER-MMPNs, as evaluated using a BCA

kit. In the FACS analysis, NIH3T6.7 cells treated with TZ-HMNCs demonstrated 46 times higher  $\Delta FI/FI_{\text{non-treated}}$  (FI: fluorescence intensity) than that of NIH3T3 cells, according to the order of the cancer marker expression level (figure 9). HER2/neu is highly expressed at the surface of NIH3T6.7 cells; NIH3T3 cells show the opposite behavior. On the other hand, IgG-HMNCs (Immunoglobulin G-conjugated HMNCs) presented hardly any cellular affinity against both cells because IgG as an irrelevant antibody has no specific binding ability for both cells.

For further confirmation of the cancer cell specific binding affinity of TZ-HMNC, microscopic images of

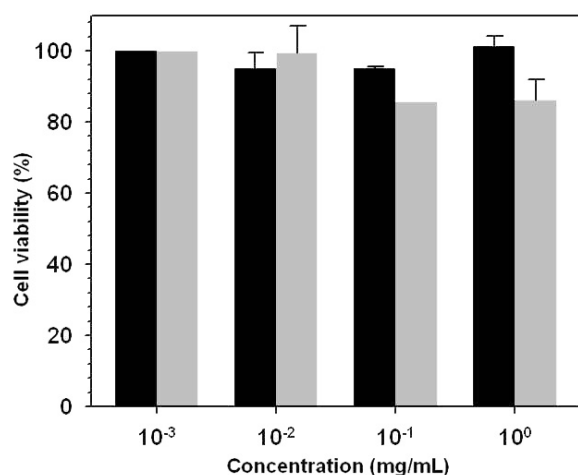


**Figure 8.** Cell viability for NIH3T3 and NIH3T6.7 cells treated with various concentrations of HMNCs by MTT assay. (NIH3T3 cells: black; NIH3T6.7 cells: gray.)

model cells were investigated. First, TZ-HMNCs and IgG-HMNCs were treated for both cells, respectively. Subsequently, fluoroisothiocyanate-labeled goat anti-human IgG as secondary antibody was attached with TZ or IgG on the surface of HMNCs for verification of the targeting ability. Moreover, the nuclear site was stained by 4',6-diamidino-2-phenylindole that demonstrated blue color. Confocal microscopic images demonstrated that TZ-HMNCs displayed excellent binding ability against NIH3T6.7 cells in comparison with NIH3T3 cells (figure 10(a)). NIH3T6.7 cells treated with TZ-HMNCs exhibited a bright green color, whereas faint green fluorescence was noted for IgG-HMNCs. Furthermore, NIH3T3 cells treated with TZ-HMNCs or IgG-HMNCs exhibited a faint green color, indicating that cellular binding affinity was low. The extent of intracellular uptake with TZ-HMNCs (or IgG-HMNCs) for both NIH3T6.7 and NIH3T3 cells was also confirmed using microscopic images after

Prussian blue staining (figure 10(b)). The transport of TZ-HMNCs into NIH3T6.7 cells took place efficiently. In contrast, NIH3T3 cells treated with TZ-HMNCs and IgG-HMNCs, and NIH3T6.7 cells treated with IgG-HMNCs exhibited insignificant cellular uptake. The small fractions of iron observed represented non-specific cellular binding of nanoparticles. Overall, FACS analysis and microscopic images demonstrated that TZ-HMNCs successfully bound to NIH3T6.7 cells and were subsequently taken up into the cells.

The targeting efficacy of TZ-HMNCs for the breast cancer cell lines were next investigated by MR imaging. In T2-weighted MR images, NIH3T6.7 cells treated with TZ-HMNCs presented black color, while NIH3T3 cells appeared as gray color (figure 11(a)). NIH3T6.7 cells incubated with TZ-HMNCs showed superior MR signal intensity ( $\Delta R2/R2_{\text{non-treated}}$ ) (figure 11(b)). The value of  $\Delta R2/R2_{\text{non-treated}}$  for NIH3T6.7 cells treated with TZ-HMNCs was 13 times higher than that of NIH3T3 cells. However both IgG-HMNC treated cells showed partial enhancement against the MR signal intensity due to non-specific binding. These results demonstrated that TZ-HMNCs have remarkable specific binding ability for cancer cells and potential as smart MR imaging agents.

#### 4. Conclusion

This study demonstrated the successful synthesis of antibody-conjugated ultrasensitive HMNCs consisting of highly sensitive magnetic nanocrystals modified with amphiphilic tri-block copolymers (PEG-PPG-PEG). The HMNCs showed excellent colloidal stability in the aqueous phase over broad ranges of pH and high salt concentration. As smart MR contrast agents, TZ-HMNCs demonstrated both excellent biocompatibility and ultrasensitive targeted detection via MRI *in vitro*. The HMNCs showed strong feasibility as efficient MR contrast agents and provide a novel strategy with potential applications to the diagnosis of cancer.

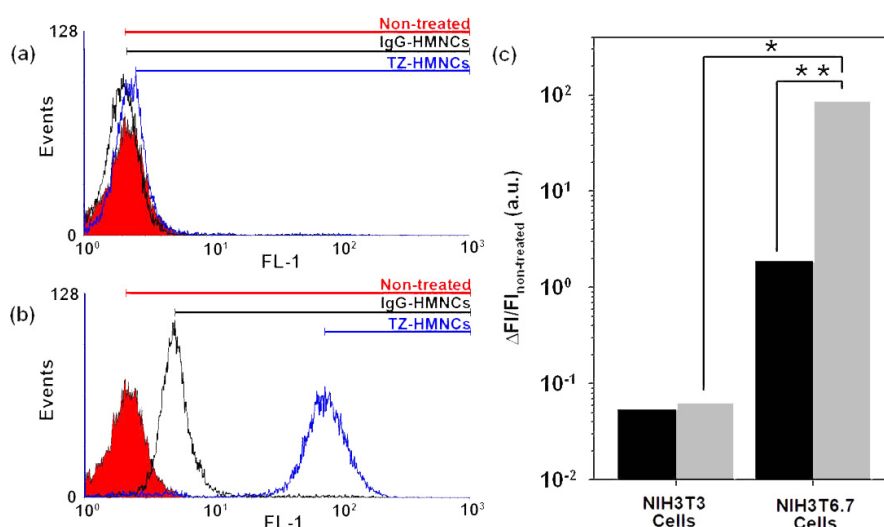


**Figure 9.** FACS analysis for (a) NIH3T3 cells and (b) NIH3T6.7 cells treated with TZ-HMNCs and IgG-HMNCs, respectively. (c) Relative fluorescence intensity ( $\Delta FI/FI_{\text{non-treated}}$ ; FI: fluorescence intensity) (IgG-HMNCs: black; TZ-HMNCs: gray) (\* and \*\*:  $p < 0.05$ ).

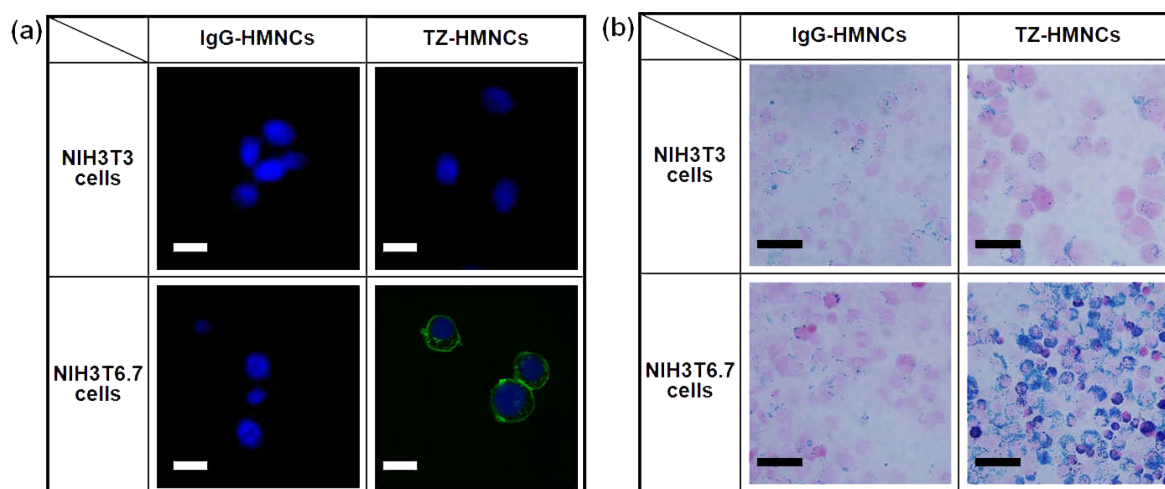


**Figure 10.** (a) Confocal microscopic images of NIH3T3 cells and NIH3T6.7 cells treated with IgG-HMNC and TZ-HMNC, respectively. The scale bars represent 200 μm. (b) Microscopic images of iron stained NIH3T3 cells and NIH3T6.7 cells treated with IgG-HMNC and TZ-HMNC. The scale bars represent 200 μm.

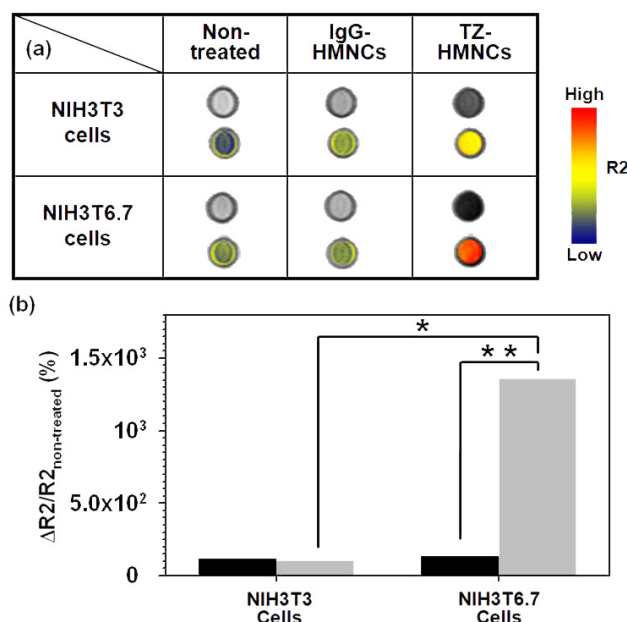


**Figure 11.** (a) The T2-weighted MR images and their color maps for NIH3T3 and NIH3T6.7 cells treated with IgG-HMNCs and TZ-HMNCs, respectively. (b) Graph of the  $\Delta R2/R2_{\text{non-treated}}$  value for NIH3T3 and NIH3T6.7 cells treated with IgG-HMNCs and TZ-HMNCs, respectively (IgG-HMNCs: black; TZ-HMNCs: gray) (\* and \*\*:  $p < 0.05$ ).

## Acknowledgments

This work was supported by a Korea Science and Engineering Foundation (KOSEF) grant funded by the Korea government (MOST) (No. M10755020001-07N5502-00110), Korea Research Foundation Grant (KRF-2005-005-J01401) and a grant from the Korea Health 21 R&D Project, Ministry of Health & Welfare, Republic of Korea (A060507).

## References

- [1] Brown M A and Semelka R C 2003 *MRI: Basic Principles and Applications* (Hoboken: Wiley-Liss)
- [2] McRobbie D W, Moore E A, Graves M J and Prince M R 2003 *MRI from Picture to Proton* (New York: Cambridge University Press)
- [3] Sosnovik D E and Weissleder R 2007 Emerging concepts in molecular MRI *Curr. Opin. Biotechnol.* **18** 4–10
- [4] Bulte J W M et al 2001 Magnetodendrimers allow endosomal magnetic labeling and *in vivo* tracking of stem cells *Nat. Biotechnol.* **19** 1141–7
- [5] McDonald D M and Choyke P L 2003 Imaging of angiogenesis: from microscope to clinic *Nat. Med.* **9** 713–25
- [6] Weissleder R, Moore A, Mahmood U, Bhorade R, Benveniste H, Chiocca E A and Basilion J P 2000 *In vivo* magnetic resonance imaging of transgene expression *Nat. Med.* **6** 351–4
- [7] Zhao M, Beauregard D A, Loizou L, Davletov B and Brindle K M 2001 Non-invasive detection of apoptosis using magnetic resonance imaging and a targeted contrast agent *Nat. Med.* **7** 1241–4
- [8] Benaron D A 2002 The future of cancer imaging *Cancer Metastasis Rev.* **21** 45–78
- [9] MARX V 2005 Molecular imaging *Chem. Eng. News* (United States: American Chemical Society) pp 25–34
- [10] Berret J F, Schonbeck N, Gazeau F, ElKharrat D, Sandre O, Vacher A and Airiau M 2006 Controlled clustering of superparamagnetic nanoparticles using block copolymers: design of new contrast agents for magnetic resonance imaging *J. Am. Chem. Soc.* **128** 1755–61
- [11] Hong C-Y, Jang I J, Horng H E, Hsu C J, Yao Y D and Yang H C 1997 Ordered structures in Fe<sub>3</sub>O<sub>4</sub> kerosene-based ferrofluids *The 41st Annual Conf. on Magnetism and Magnetic Materials* (Atlanta, GA: AIP) pp 4275–7
- [12] Fried T, Shemer G and Markovich G 2001 Ordered two-dimensional arrays of ferrite nanoparticles *Adv. Mater.* **13** 1158–61
- [13] Jeong U, Teng X, Wang Y, Yang H and Xia Y 2007 Superparamagnetic colloids: controlled synthesis and niche applications *Adv. Mater.* **19** 33–60
- [14] Park J, Joo J, Kwon S G, Jang Y and Hyeon T 2007 Synthesis of monodisperse spherical nanocrystals *Angew. Chem. Int. Edn* **46** 4630–60



- [15] Hyeon T 2003 Chemical synthesis of magnetic nanoparticles *Chem. Commun.* **927–34**
- [16] Kang Y S, Risbud S, Rabolt J F and Stroeve P 1996 Synthesis and characterization of nanometer-size  $\text{Fe}_3\text{O}_4$  and  $\gamma\text{-Fe}_2\text{O}_3$  particles *Chem. Mater.* **8** 2209–11
- [17] Sun S and Zeng H 2002 Size-controlled synthesis of magnetite nanoparticles *J. Am. Chem. Soc.* **124** 8204–5
- [18] Sun S, Zeng H, Robinson D B, Raoux S, Rice P M, Wang S X and Li G 2004 Monodisperse  $\text{MFe}_2\text{O}_4$  ( $\text{M} = \text{Fe}, \text{Co}, \text{Mn}$ ) nanoparticles *J. Am. Chem. Soc.* **126** 273–9
- [19] Park J, An K, Hwang Y, Park J-G, Noh H-J, Kim J-Y, Park J-H, Hwang N-M and Hyeon T 2004 Ultra-large-scale syntheses of monodisperse nanocrystals *Nat. Mater.* **3** 891–5
- [20] Ai H, Flask C, Weinberg B, Shuai X T, Pagel M D, Farrell D, Duerk J and Gao J 2005 Magnetite-loaded polymeric micelles as ultrasensitive magnetic-resonance probes *Adv. Mater.* **17** 1949–52
- [21] Yang J, Lee C-H, Ko H-J, Suh J-S, Yoon H-G, Lee K, Huh Y-M and Haam S 2007 Multifunctional magneto-polymeric nanohybrids for targeted detection and synergistic therapeutic effects on breast cancer *Angew. Chem. Int. Edn* **46** 8836–9
- [22] Yang J *et al* 2007 Synthesis of ultrasensitive magnetic resonance contrast agents for cancer imaging using PEG-Fatty acid *Chem. Mater.* **19** 3870–6
- [23] Huh Y M *et al* 2005 *In vivo* magnetic resonance detection of cancer by using multifunctional magnetic nanocrystals *J. Am. Chem. Soc.* **127** 12387–91
- [24] Jun Y w *et al* 2005 Nanoscale size effect of magnetic nanocrystals and their utilization for cancer diagnosis via magnetic resonance imaging *J. Am. Chem. Soc.* **127** 5732–3
- [25] Lee J-H *et al* 2007 Artificially engineered magnetic nanoparticles for ultra-sensitive molecular imaging *Nat. Med.* **13** 95–9
- [26] Malmsten M 2002 *Surfactants and Polymers in Drug Delivery* (New York: Dekker)
- [27] Harris J M 1992 *Poly(ethylene glycol) Chemistry: Biotechnical and Biomedical Applications* (New York: Plenum)
- [28] Veronese F M and Pasut G 2005 PEGylation, successful approach to drug delivery *Drug Discov. Today* **10** 1451–8
- [29] Yu W W, Chang E, Falkner J C, Zhang J, Al-Somali A M, Sayes C M, Johns J, Drezek R and Colvin V L 2007 Forming biocompatible and nonaggregated nanocrystals in water using amphiphilic polymers *J. Am. Chem. Soc.* **129** 2871–9
- [30] Nasongkla N, Bey E, Ren J, Ai H, Khemtong C, Guthi J S, Chin S F, Sherry A D, Boothman D A and Gao J 2006 Multifunctional polymeric micelles as cancer-targeted, MRI-ultrasensitive drug delivery systems *Nano Lett.* **6** 2427–30
- [31] Gao X, Cui Y, Levenson R M, Chung L W K and Nie S 2004 *In vivo* cancer targeting and imaging with semiconductor quantum dots *Nat. Biotechnol.* **22** 969–76
- [32] Gonzales M and Krishnan K M 2007 Phase transfer of highly monodisperse iron oxide nanocrystals with Pluronic F127 for biomedical applications *J. Magn. Magn. Mater.* **311** 59–62
- [33] Jain T K, Morales M A, Sahoo S K, Leslie-Pelecky D L and Labhasetwar V 2005 Iron oxide nanoparticles for sustained delivery of anticancer agents *Mol. Pharm.* **2** 194–205
- [34] Hermanson G T 1996 *Bioconjugate Techniques* (San Diego, CA: Academic)
- [35] Bae Y H, Huh K M, Kim Y and Park K-H 2000 Biodegradable amphiphilic multiblock copolymers and their implications for biomedical applications *J. Control. Release* **64** 3–13
- [36] Mundargi R C, Srirangarajan S, Agnihotri S A, Patil S A, Ravindra S, Setty S B and Aminabhavi T M 2007 Development and evaluation of novel biodegradable microspheres based on poly(d,l-lactide-co-glycolide) and poly([epsilon]-caprolactone) for controlled delivery of doxycycline in the treatment of human periodontal pocket: *in vitro* and *in vivo* studies *J. Control. Release* **119** 59–68